



Article

Low Overpotential Amperometric Sensor Using $\text{Yb}_2\text{O}_3\cdot\text{CuO@rGO}$ Nanocomposite for Sensitive Detection of Ascorbic Acid in Real Samples

Jahir Ahmed ^{1,2} , Mohd Faisal ^{1,2}, Jari S. Algethami ^{1,2} , Mabkhoot A. Alsaieri ^{1,3}, Saeed A. Alsareii ^{1,4} and Farid A. Harraz ^{1,3,*}

¹ Promising Centre for Sensors and Electronic Devices (PCSED), Advanced Materials and Nano-Research Centre, Najran University, Najran 11001, Saudi Arabia; janurulislam@nu.edu.sa (J.A.); mfahsan@nu.edu.sa (M.F.); jsalgethami@nu.edu.sa (J.S.A.); mamalsaiari@nu.edu.sa (M.A.A.); alsareii@nu.edu.sa (S.A.A.)

² Department of Chemistry, Faculty of Science and Arts, Najran University, Najran 11001, Saudi Arabia

³ Department of Chemistry, Faculty of Science and Arts at Sharurah, Najran University, Sharurah 68342, Saudi Arabia

⁴ Department of Surgery, College of Medicine, Najran University, Najran 11001, Saudi Arabia

* Correspondence: faharraz@nu.edu.sa

Abstract: The ultimate objective of this research work is to design a sensitive and selective electrochemical sensor for the efficient detection of ascorbic acid (AA), a vital antioxidant found in blood serum that may serve as a biomarker for oxidative stress. To achieve this, we utilized a novel $\text{Yb}_2\text{O}_3\cdot\text{CuO@rGO}$ nanocomposite (NC) as the active material to modify the glassy carbon working electrode (GCE). The structural properties and morphological characteristics of the $\text{Yb}_2\text{O}_3\cdot\text{CuO@rGO}$ NC were investigated using various techniques to ensure their suitability for the sensor. The resulting sensor electrode was able to detect a broad range of AA concentrations (0.5–1571 μM) in neutral phosphate buffer solution, with a high sensitivity of $0.4341 \mu\text{A} \mu\text{M}^{-1} \text{cm}^{-2}$ and a reasonable detection limit of 0.062 μM . The sensor's great sensitivity and selectivity allowed it to accurately determine the levels of AA in human blood serum and commercial vitamin C tablets. It demonstrated high levels of reproducibility, repeatability, and stability, making it a reliable and robust sensor for the measurement of AA at low overpotential. Overall, the $\text{Yb}_2\text{O}_3\cdot\text{CuO@rGO}$ /GCE sensor showed great potential in detecting AA from real samples.

Keywords: ascorbic acid; amperometric sensor; $\text{Yb}_2\text{O}_3\cdot\text{CuO@rGO}$; vitamin C; human blood serum



Citation: Ahmed, J.; Faisal, M.; Algethami, J.S.; Alsaieri, M.A.; Alsareii, S.A.; Harraz, F.A. Low Overpotential Amperometric Sensor Using $\text{Yb}_2\text{O}_3\cdot\text{CuO@rGO}$ Nanocomposite for Sensitive Detection of Ascorbic Acid in Real Samples. *Biosensors* **2023**, *13*, 588. <https://doi.org/10.3390/bios13060588>

Received: 7 April 2023

Revised: 20 May 2023

Accepted: 24 May 2023

Published: 29 May 2023



Copyright: © 2023 by the authors. Licensee MDPI, Basel, Switzerland. This article is an open access article distributed under the terms and conditions of the Creative Commons Attribution (CC BY) license (<https://creativecommons.org/licenses/by/4.0/>).

1. Introduction

Ascorbic acid (AA) is a vital biomolecule that is present in a variety of naturally occurring sources, including fruits and vegetables, and that functions as a nutrient and antioxidant [1]. It is essential to numerous bodily metabolic activities including activating the immune system, aiding in wound healing, helping with the absorption of iron, and protecting against damage to bones and teeth [2]. Additionally, AA serves as a cofactor during the synthesis of collagen and carnitine [3]. In addition, AA has been demonstrated to provide protective effects against oxidative illnesses such as heart disease, several cancers, AIDS, the common cold, etc. [4]. However, there is no AA produced by the human body and it can only be obtained through the consumption of foods and medicines [5]. AA is a crucial ingredient in dietary and pharmaceutical supplements [6]. Human blood serum typically contains between 28.5 and 85.2 μM of AA, and the amount of AA in blood serum can provide information about a person's general state of health [7]. Scurvy and anemia can result from an AA deficit in blood serum, while an excess of AA can lead to gastric irritation or diarrhea [8]. Therefore, it is crucial to have precise and efficient techniques for figuring out how much AA is present in foods, medications, and blood serum.

Direct titration [9], chromatography [10], spectrophotometry [11], and solid-phase spectrophotometry [12] are currently used methods for AA measurement. However, such methods are costly and require skilled personnel as well as challenging analytical measures for multi-sample preparation. To address these issues, researchers are working to develop efficient and cost-effective methods for real-time and in situ AA determination. The advantages of electrochemical detection include quicker measurements, reduced sample size, reduced costs, and an absence of pre-concentration processes, making them handy, portable, and simple to use with miniaturized electrodes [13]. However, due to its irreversible nature and high overpotential requirements, the electrochemical AA oxidation at a bare electrode might have negative effects on selectivity, electrode fouling, and repeatability. Therefore, it is indispensable to fabricate an electrode surface that enables efficient AA detection with less overpotential. In recent years, to detect AA, researchers have proposed several sensors, including electrodes modified with metals and metal oxides [14], alkylimidazolium salt [15], graphene derivatives [16], carbon nanotubes [14], and polymers [17].

Due to their potential technological uses and intriguing optical and structural characteristics, semiconducting doped nanostructured materials comprising transition metal oxides have drawn a lot of attention. Due to their size, shape, and surface, these materials have distinct physical and chemical properties that make them relevant in a variety of study fields and applications for industry. In particular, metal oxide-based sensors have been explored for their diverse uses in areas such as the protection of the environment, chemical process management, personal security, healthcare, and in the military [18–20]. These sensors have several advantages, including their compact size, affordable price, lower power consumption, straightforward processing, and good stability [21]. Previously, researchers have investigated various types of metal oxides, such as CuO [22,23], MnO₂ [24], NiO [25], Fe₂O₃ [26], and ZnO [27], as electron mediators for sensing applications. Additionally, doped metal oxides, such as NiO.CoO nanocomposites [28], CdO.SnO₂.V₂O₅ [29], CuO.In₂O₃ [30], CuO.Nd₂O₅ [31], CuO.NiO [32], and CuO.ZnO [33], have been studied as efficient sensing materials with higher sensitivity, small detection limits, wide linear dynamic ranges, and quick response times. CuO, a *p*-type semiconductor, has shown particularly good performance as an electrocatalyst in sensing applications [34]. To improve the performance of CuO, researchers have also investigated using other semiconductor metal oxides such as In₂O₃ [30], Nd₂O₅ [31], NiO [32], TiO₂ [35], and SnO₂ [36] in combination with CuO as bimetallic oxide pairs. Ytterbium oxide (Yb₂O₃) has also been explored for use in sensing applications [37–39]. Yb₂O₃ is a lanthanide-based C-type sesquioxide that can exhibit electrochemical redox characteristics [40]. In addition, the electrical as well as structural and morphological properties of the CuO can be engineered through doping of the CuO matrix with suitable dopants. Many trivalent lanthanide ions and their oxides have been reported as excellent dopants for CuO with modified and enhanced electrical properties. However, a detailed literature survey revealed very few reports for the synthesis of Yb₂O₃-doped CuO structures. Thus, here we have synthesized the Yb₂O₃-doped CuO nanostructures through the coprecipitation method. Furthermore, this Yb₂O₃.CuO was combined with rGO to obtain the ternary Yb₂O₃.CuO@rGO nanocomposite for the AA sensing with improved sensor parameters.

A lot of research has been carried out on the applicability of carbonaceous nanomaterials for sensing applications, including reduced graphene oxide, activated carbon, mesoporous carbon, and carbon nanotubes. In particular, graphene, a sheet of sp²-bonded carbon atoms, with a particular surface area, low density, outstanding electrical conductivity, and great mechanical properties, has drawn a lot of interest [41,42]. Graphene-based 3D nanomaterials have also generated huge interest due to their high surface area, lower density, better electrical conductivity, and exceptional mechanical properties [43,44]. Composite materials made of metal oxides and graphene have recently been explored for their stability, long-term storage, and photo-catalytic capabilities [45,46]. Many graphene-based nanomaterials have been studied in sensing applications [47–49]. However, rare earth oxide-transition metal oxide-reduced graphene nanocomposite has hardly been studied in

sensing applications. Hence, in this work, we developed and examined Yb₂O₃.CuO@rGO nanocomposite (NC) as the active sensing material for AA detection.

Inspired by previous works available in the literature, we synthesized Yb₂O₃-doped CuO nanoparticles to improve stability, sensitivity, and selectivity, and then used a simple sonication technique to synthesize the Yb₂O₃.CuO@rGO NC sensing material. This study presents a simple method for preparing an electrochemical AA sensor using Yb₂O₃.CuO@rGO NC that offered improved selectivity and sensitivity. As far as we are aware, this will be the maiden article utilizing Yb₂O₃.CuO@rGO NC to develop an enzyme-less AA electrochemical sensor.

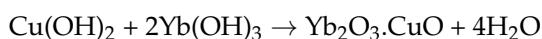
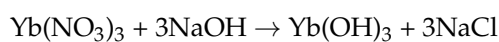
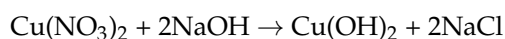
2. Materials and Methods

2.1. Materials

All necessary chemicals, including ascorbic acid, copper (II) nitrate, ytterbium (III) nitrate, sodium hydroxide, reduced graphene oxide, NaH₂PO₄, Na₂HPO₄, citric acid, glucose, uric acid, dopamine, sodium chloride, and calcium nitrate, were purchased from Sigma–Aldrich, and utilized exactly as they were given. All solutions were made using double-distilled water. The XPS investigation of Yb₂O₃.CuO@rGO was performed using a MgKα spectrometer (JEOL, JPS 9200) in the subsequent circumstances: pass energy = 50 eV (wide-scan) and 30 eV (narrow-scan), Voltage = 10 kV, Current = 20 mA. A PANalytical X-ray diffractometer was used to acquire X-ray diffraction (XRD) spectra with Cu Kα_{1/2}, λ_{α₁} = 154.060 pm, λ_{α₂} = 154.439 pm radiation. A “Raman station 400 (Perkin Elmer)” spectrometer was used to acquire the Raman spectra. A FE-SEM (JEOL-6300F, 5 kV) was used to analyze the morphology and structural characteristics of Yb₂O₃.CuO@rGO. EDS (JEOL) was used to investigate the elemental composition of the Yb₂O₃.CuO@rGO. A JEOL JEM-2100F-UHR field emission apparatus fitted with a Gatan GIF 2001 energy filter and a 1 k-CCD camera was used to capture transmission electron microscopy (TEM) micrographs at 200 kV. Electrochemical measurements were conducted using a Zahner Zennium potentiostat.

2.2. Synthesis of CuO, Yb₂O₃, Yb₂O₃.CuO, and Yb₂O₃.CuO@rGO Nanocomposite

To synthesize the CuO, Yb₂O₃, Yb₂O₃.CuO, and Yb₂O₃.CuO@rGO nanocomposites, the following process was followed: firstly, equimolar Cu(NO₃)₂ and Yb(NO₃)₃ solutions were mixed in a beaker and stirred for half an hour at 70 °C. This mixture was then combined with NaOH and stirred vigorously at 80 °C for 8 h. Afterwards, the ensuing dark precipitate was cleaned with distilled water and ethanol to remove contaminants and the resulting black precipitate was dried at 80 °C. This as-grown Yb₂O₃.CuO nanoparticle (NP) was then calcined by heating it for six hours at 500 °C in a furnace. During this synthesis process, the following chemical reactions occurred:



Precursors, Yb³⁺ and Cu²⁺ ions are soluble in NaOH solution, where NaOH keeps the pH constant during the reaction and continuously releases OH[−]. The development of the Cu(OH)₂ nucleus starts when the ionic product of Cu²⁺ and OH[−] exceeds the K_{sp} value. Similarly, Yb(OH)₃ was also produced. Cu²⁺ ions easily incorporate themselves into the Yb₂O₃ lattice because of the similar ionic radii. On heating, hydroxides decompose to produce respective oxides. Similarly, CuO and Yb₂O₃ NPs were also synthesized.

To synthesize the $\text{Yb}_2\text{O}_3\cdot\text{CuO}@r\text{GO}$ nanocomposite, 0.5 g of $\text{Yb}_2\text{O}_3\cdot\text{CuO}$ NPs and 0.025 g of reduced graphene oxide (rGO) were mixed followed by 40 min of sonication in 80 mL distilled water. This resulting mixture was then filtered and had 12 h of drying in an oven at 70 °C.

2.3. Glassy Carbon Electrode Modification Using $\text{Yb}_2\text{O}_3\cdot\text{CuO}@r\text{GO}$ Nanocomposite

Glassy carbon electrodes (GCEs) (diameter = 3 mm; BAS Inc., Sumida-Ku, Japan) were cleaned using a 1 μm diamond past, followed by a 0.05 μm alumina slurry using the commercially available polishing pads. Next, the GCE was fabricated utilizing $\text{Yb}_2\text{O}_3\cdot\text{CuO}@r\text{GO}$ nanocomposite using a Nafion solution. During the fabrication process, 4.0 mg of $\text{Yb}_2\text{O}_3\cdot\text{CuO}@r\text{GO}$ was uniformly mixed with 0.05 mL Nafion and 0.45 mL propan-2-ol, and then 2 μL of this suspension was carefully applied to a pre-cleaned GCE and dried at 60 °C for 20 min. Such a fabricated GCE was labeled as the $\text{Yb}_2\text{O}_3\cdot\text{CuO}@r\text{GO}/\text{GCE}$. Control experiments were also conducted, in which CuO/GCE , $\text{Yb}_2\text{O}_3/\text{GCE}$, $r\text{GO}/\text{GCE}$, and $\text{Yb}_2\text{O}_3\cdot\text{CuO}/\text{GCE}$ were fabricated using similar procedures. The electrochemical investigations of AA (0.5–1744 μM) were carried out in a typical three-electrode electrochemical cell at ambient conditions in 0.1 M PBS (pH 7.0), a $\text{Yb}_2\text{O}_3\cdot\text{CuO}@r\text{GO}/\text{GCE}$, Ag/AgCl , and a platinum spiral were served as the working, reference, and counter electrodes, respectively.

3. Results and Discussion

3.1. Characterization of $\text{Yb}_2\text{O}_3\cdot\text{CuO}@r\text{GO}$ Nanocomposite

The elemental compositions and structure of $\text{Yb}_2\text{O}_3\cdot\text{CuO}@r\text{GO}$ were examined using XPS. It is evident from the XPS analysis shown in Figure 1a–e that $\text{Yb}_2\text{O}_3\cdot\text{CuO}@r\text{GO}$ nanocomposite is composed of Yb, Cu, O, and C atoms only. The $\text{Yb}4d_{5/2}$ spectrum has three clearly defined peaks appearing at energies of 187.2, 188.4, and 189.1, which are compatible with $\text{Yb}4d$ (Figure 1b) [50]. In the deconvoluted $\text{Cu}2p$ spectrum in Figure 1c, there are two peaks at 937.1 and 956.8 eV that may be related to $\text{Cu}2p_{3/2}$ and $\text{Cu}2p_{1/2}$, respectively [51]. In between these two peaks, there are some satellite peaks that appeared that are also consistent with the literature [52]. Figure 1d shows two peaks from the fine-scan O1s spectra that are associated with the Yb–O and Cu–O bonds, respectively, at 533.3 and 535.2 eV [13]. Three peaks are shown in the fine-scan C1s spectrum in Figure 1e at energies of 284.6, 287.2, and 289.1 eV. The peaks at 284.6 and 287.2 eV may be attributed to C–C and C–O–H bonds, respectively [53], and the remaining peak at 289.1 eV can be correlated to COOH [54].

XRD patterns in Figure 2a showed diffraction bands at $2\theta = 20.80, 29.50, 34.30, 36.50, 40.60, 44.00, 47.50, 49.20, 51.00, 54.10, 57.10, 58.50, 60.00$, and 61.50 , which are related to the (211), (222), (400), (411), (332), (134), (125), (440), (443), (611), (145), (662), (136), and (444) planes for Yb_2O_3 NPs (JCPDS#65-3173), respectively [50]. The diffraction bands at $35.40, 38.60, 48.60, 58.20, 61.60, 66.30$, and 68.10 can be related to (002), (111), (−202), (202), (−113), (−311), and (220) planes of CuO NPs (JCPDS#45-0937), respectively [55]. The $\text{Yb}_2\text{O}_3\cdot\text{CuO}@r\text{GO}$ contains the rGO peak connected to carbon that is often appearing at $2\theta = 24.30$ which is correlated to (002) plane [56] but is not easily visible in Figure 2a due to low intensity. However, the presence of carbon in $\text{Yb}_2\text{O}_3\cdot\text{CuO}@r\text{GO}$ was established by XPS, EDS, SEM, and TEM. Figure 2b shows the Raman spectra, where bands at $359.3, 718$, and 1060 cm^{-1} can be related to Yb_2O_3 , while bands at 328 and 850 cm^{-1} were connected to CuO [57]. The characteristic carbon bands at 1344 and 1676 cm^{-1} are related to the D and G bands of rGO [58].

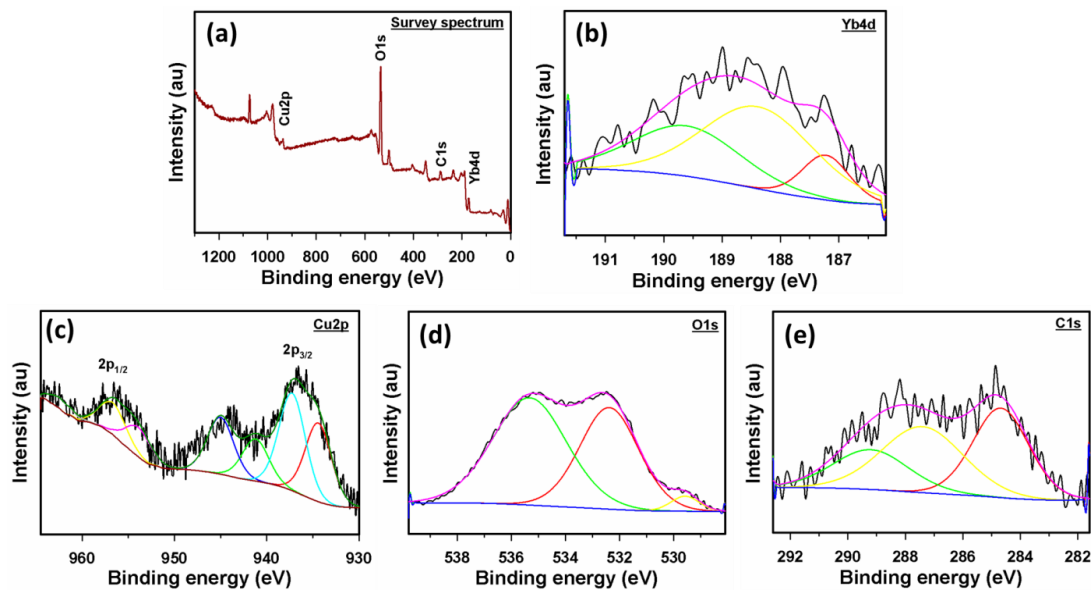


Figure 1. (a) Survey XPS spectrum of $\text{Yb}_2\text{O}_3.\text{CuO}@r\text{GO}$ NC, (b) deconvoluted spectra of Yb4d, (c) Cu2p, (d) O1s, and (e) C1s of $\text{Yb}_2\text{O}_3.\text{CuO}@r\text{GO}$ nanocomposite.

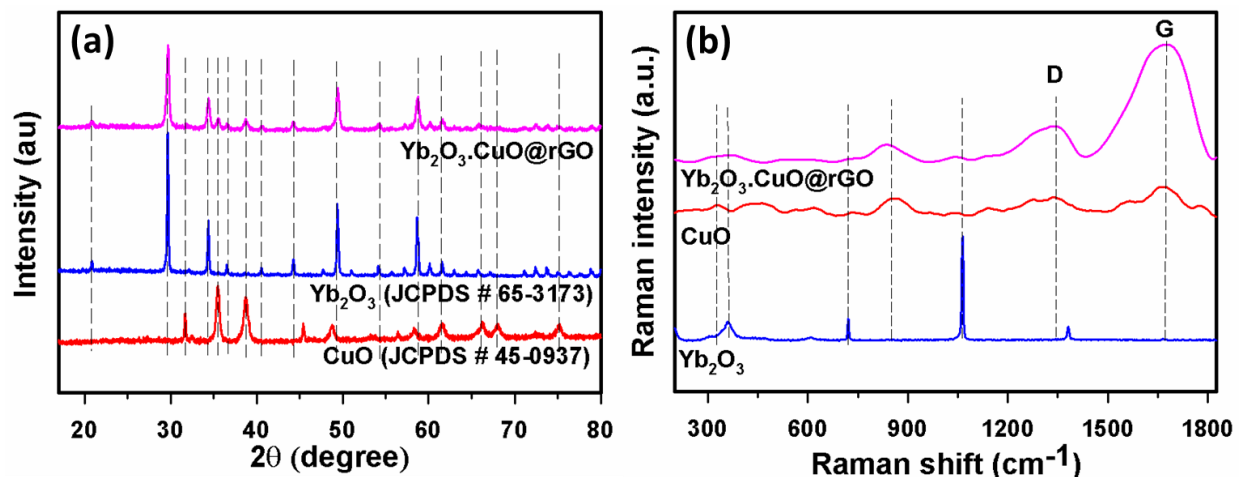


Figure 2. (a) XRD patterns and (b) Raman spectra of CuO, Yb_2O_3 , and $\text{Yb}_2\text{O}_3.\text{CuO}@r\text{GO}$ NC.

FESEM was employed to analyze the morphological and surface structure of CuO, Yb_2O_3 , $\text{Yb}_2\text{O}_3.\text{CuO}$, and $\text{Yb}_2\text{O}_3.\text{CuO}@r\text{GO}$ nanocomposite as presented in Figure 3a–d. The $\text{Yb}_2\text{O}_3.\text{CuO}@r\text{GO}$ nanocomposite was found to be made up of $\text{Yb}_2\text{O}_3.\text{CuO}$ composites that were randomly distributed over the graphene sheets. EDS was used to determine the $\text{Yb}_2\text{O}_3.\text{CuO}@r\text{GO}$ nanocomposite's elemental composition (Figure 3e), and the results showed that the nanocomposite is exclusively made of Yb, Cu, O, and C with their respective weight percentages as 39.37%, 17.02%, 29.27%, and 14.34%. This elemental composition agrees with the findings of XPS and XRD. A more thorough morphology of CuO, Yb_2O_3 , $\text{Yb}_2\text{O}_3.\text{CuO}$, and $\text{Yb}_2\text{O}_3.\text{CuO}@r\text{GO}$ nanocomposite was provided by the TEM images in Figure 3f–i that show a collection of spherical Yb_2O_3 and elongated CuO NPs dispersed on sheet-like structures of rGO. Figure 3j presents an HR-TEM image of the $\text{Yb}_2\text{O}_3.\text{CuO}@r\text{GO}$ nanocomposite and Figure 3k displays the selected area electron diffraction (SAED) patterns, which unequivocally reveal that the composite is polycrystalline.

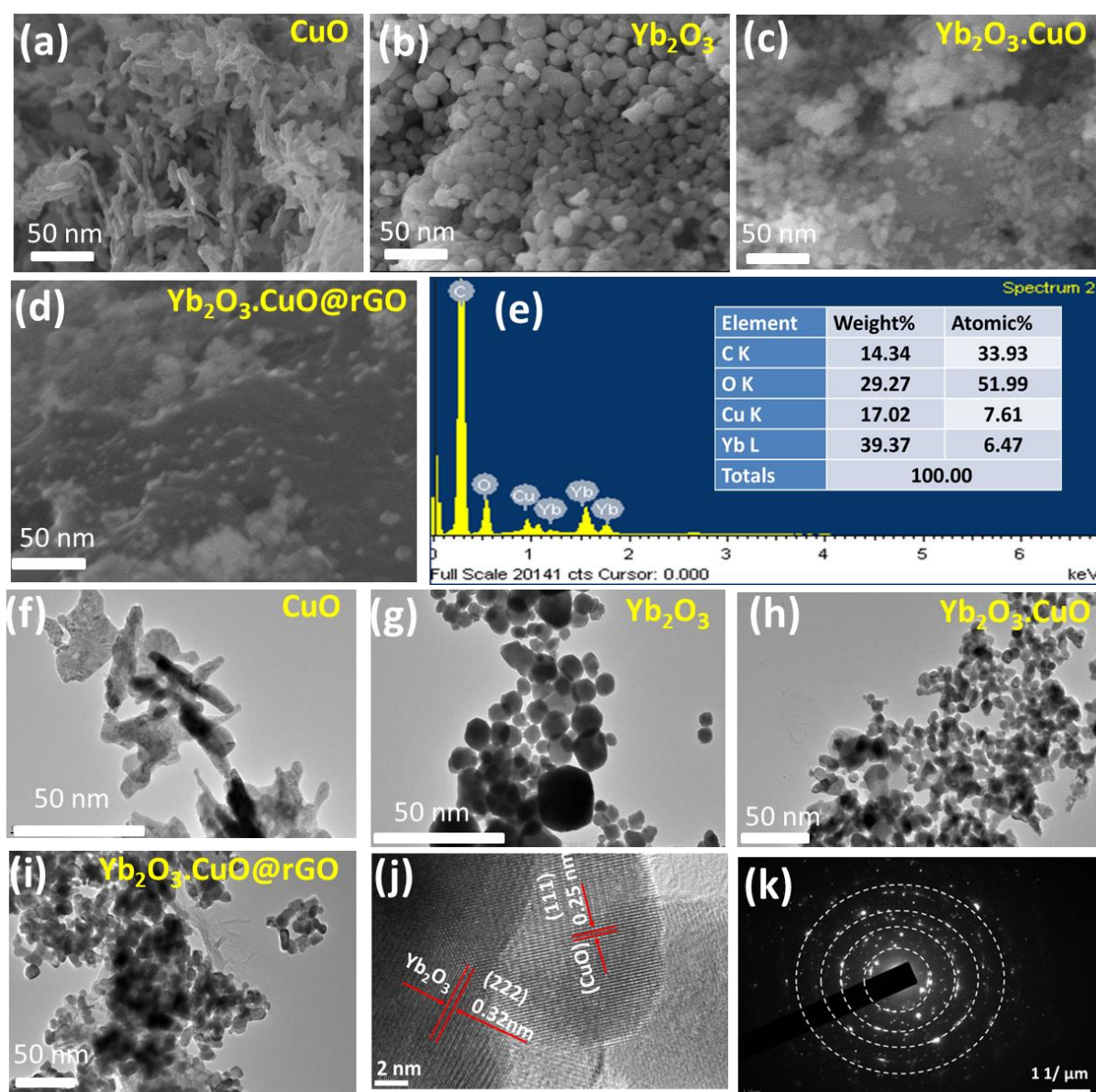


Figure 3. FESEM image: (a) CuO, (b) Yb₂O₃, (c) Yb₂O₃.CuO, (d) Yb₂O₃.CuO@rGO, (e) EDS spectrum of Yb₂O₃.CuO@rGO; TEM micrograph from (f) CuO, (g) Yb₂O₃, (h) Yb₂O₃.CuO, (i) Yb₂O₃.CuO@rGO, (j) HR-TEM image, and (k) SAED patterns of Yb₂O₃.CuO@rGO nanocomposite.

3.2. Ascorbic Acid Sensor Development

3.2.1. Electrochemical Study of Yb₂O₃.CuO@rGO/GCE Assembly

We evaluated the electro-chemical activity of the modified electrodes through cyclic voltammetry (CV) and electrochemical impedance spectroscopy (EIS). Figure 4a illustrates the feeble CV response from a bare GCE in the presence of 40 μM AA at +0.52 V; however, the CuO/GCE and Yb₂O₃.CuO/GCE showed enhanced CV outputs at +0.41 V and 0.28 V, respectively. For the Yb₂O₃/GCE and rGO/GCE electrodes, no CV response was detected. A significantly improved CV result at a low potential of +0.25 V was obtained from the Yb₂O₃.CuO@rGO/GCE. This demonstrates that this Yb₂O₃.CuO@rGO/GCE assembly possessed the greatest electrocatalytic performance during AA determination in comparison to other the electrodes shown in Figure 4a. Therefore, we designated the Yb₂O₃.CuO@rGO/GCE assembly as an AA sensor in this investigation. Additionally, a definite CV peak was produced for the Yb₂O₃.CuO@rGO/GCE sensor with 40 μM AA while, in the absence of AA, no CV response was seen (Figure 4b), further emphasizing the

effective electro-chemical properties of $\text{Yb}_2\text{O}_3\cdot\text{CuO@rGO}/\text{GCE}$ as an AA sensor. Figure 4c displays EIS Nyquist plots of bare GCE, CuO/GCE , $\text{Yb}_2\text{O}_3/\text{GCE}$, $\text{Yb}_2\text{O}_3\cdot\text{CuO}/\text{GCE}$, and $\text{Yb}_2\text{O}_3\cdot\text{CuO@rGO}/\text{GCE}$, and a relevant equivalent circuit is presented in the inset. The $\text{Yb}_2\text{O}_3\cdot\text{CuO@rGO}/\text{GCE}$ electrode was found to have the shortest semicircle diameter, which indicates that its charge transfer resistance ($R_{ct} = 9.2 \text{ k}\Omega$) value is lower than that of other electrodes including bare GCE ($75.2 \text{ k}\Omega$), CuO/GCE ($35.2 \text{ k}\Omega$), $\text{Yb}_2\text{O}_3/\text{GCE}$ ($94.7 \text{ k}\Omega$), and $\text{Yb}_2\text{O}_3\cdot\text{CuO}/\text{GCE}$ ($22.9 \text{ k}\Omega$), which were acquired through fitting utilizing the EIS Spectrum Analyzer Software. The smallest semicircular diameter of the $\text{Yb}_2\text{O}_3\cdot\text{CuO@rGO}/\text{GCE}$ electrode suggests that the fabrication process lowered its R_{ct} value. We therefore draw the conclusion that the $\text{Yb}_2\text{O}_3\cdot\text{CuO@rGO}/\text{GCE}$ electrode provided improved electron transfer performance than the other modified electrodes shown in Figure 4a.

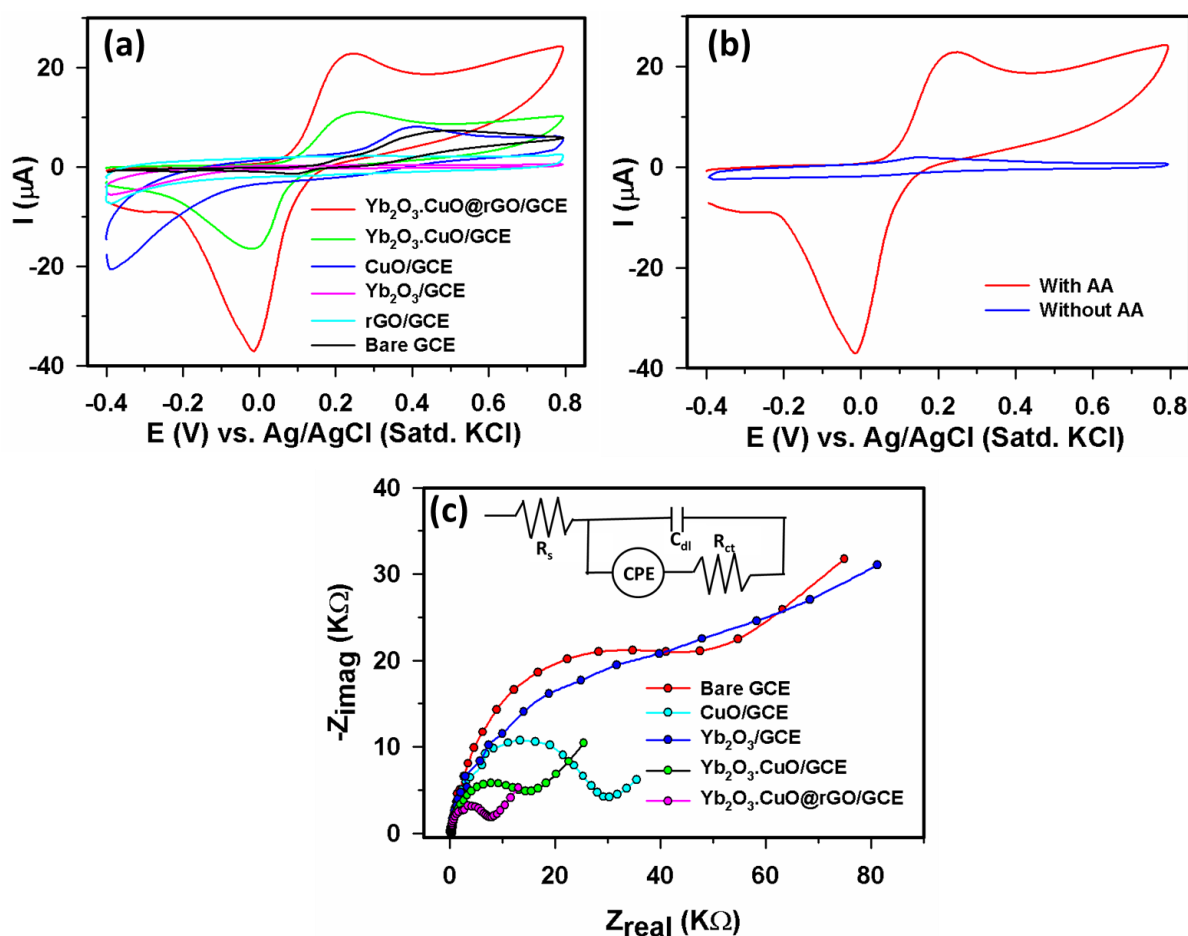


Figure 4. CVs recorded at scan rate 0.05 V s^{-1} in 0.1 M PBS (pH 7.0) (a) CVs from bare GCE, CuO/GCE , $\text{Yb}_2\text{O}_3/\text{GCE}$, rGO/GCE , $\text{Yb}_2\text{O}_3\cdot\text{CuO}/\text{GCE}$, $\text{Yb}_2\text{O}_3\cdot\text{CuO@rGO}/\text{GCE}$ with 40 μM AA, (b) CVs from the $\text{Yb}_2\text{O}_3\cdot\text{CuO@rGO}/\text{GCE}$ with 40 μM AA and without AA, and (c) EIS Nyquist plots acquired using various electrodes in 1.0 mM $[\text{Fe}(\text{CN})_6]^{3-/4-}$ in 0.1 M KCl at +0.50 V, at signal amplitude 10 mV, and with frequency ranging from 0.1 Hz to 100 KHz with a relevant equivalent circuit in the inset.

We investigated the impact of a pH between 6.0 and 8.0 with 40 μM AA to better understand the electrochemical AA oxidation. Figure 5a,b shows that, for a pH of 6.0 to 7.0, the anodic peak current (I_{pa}) value steadily increased and, for a pH 7.0 to 8.0, a declining trend was seen. The extreme I_{pa} was seen at a pH ~ 7.0 , as shown in Figure 5b. As a result, pH 7.0 was set as the standard for the remaining tests in this paper. Figure 5c displayed a straight-line plot for anodic peak potential (E_{pa}) vs. pH having a regression Equation (1):

$$E_{pa}(\text{V}) = 0.5614 - 0.0467\text{pH} \quad (R^2 = 0.9750) \quad (1)$$

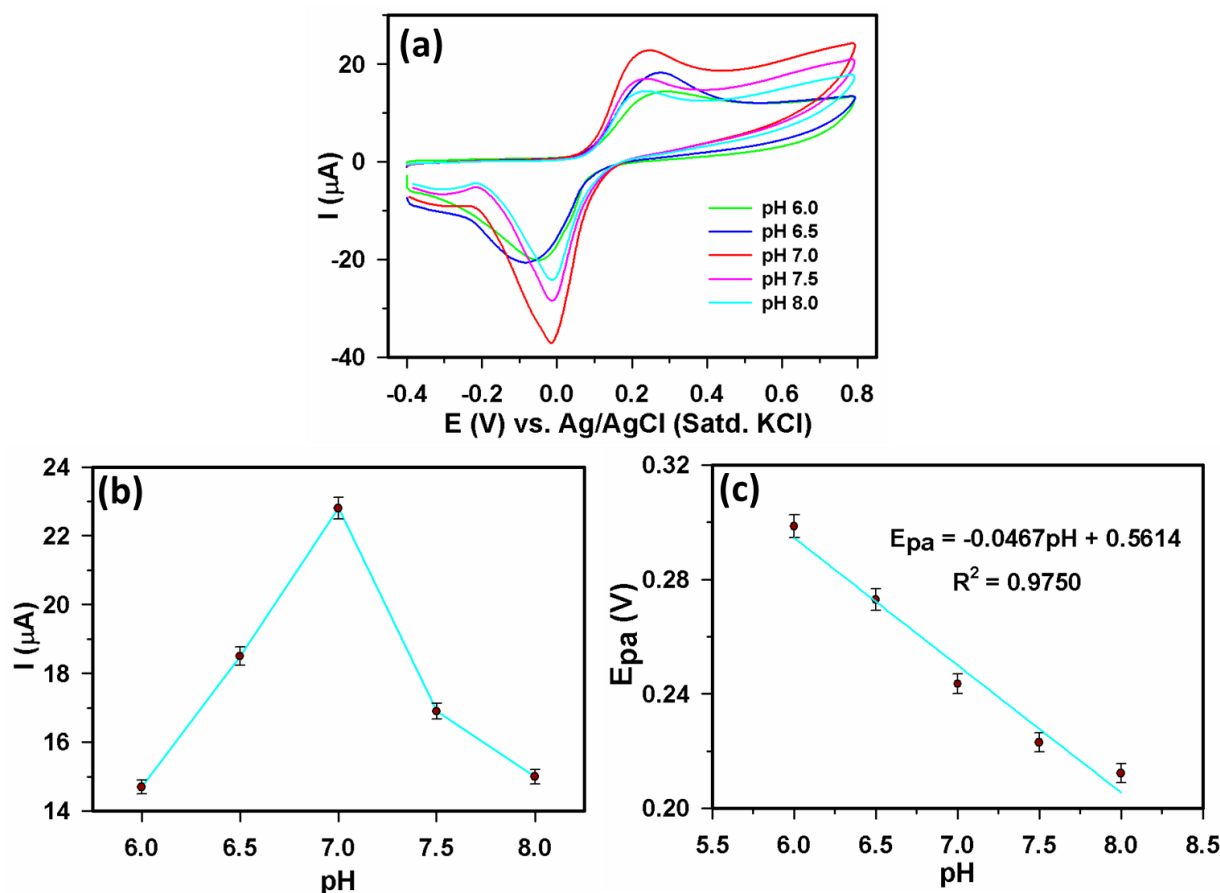


Figure 5. (a) CVs recorded using 40 μM AA in 0.1 M PBS at varying pH (6.0–8.0) at 0.05 V s⁻¹ scan rate, (b) I_{pa} vs. pH, and (c) E_{pa} vs. pH.

Figure 5c showed that the gradient of −56 mV per pH unit over the selected pH range is extremely near to the predicted value of −59, demonstrating that the quantity of transported protons and electrons involved in this AA oxidation are equal [13,19].

Scan rate (v) analysis in Figure 6a shows the CVs of 40 μM AA acquired using different scan rates (20–200 mV s⁻¹) using a Yb₂O₃.CuO@rGO/GCE sensor. The I_{pa} value in Figure 6a was rising as v increased, although the E_{pa} value only marginally changed in a positive way. The nonlinear change in I_{pa} vs. v in Figure 6b suggested that AA oxidation is not a surface-controlled process [59] while, in Figure 6c, a linear I_{pa} vs. $v^{1/2}$ curve was seen, validating a diffusion-controlled process [60] using Equation (2) below.

$$I_{pa}(\mu A) = 190.3043 v^{1/2} (V^{1/2} s^{-1/2}) - 9.5808 \quad (R^2 = 0.9978) \quad (2)$$

Additionally, in Figure 6d, a straight line from E_{pa} vs. log(v) plot was seen using Equation (3).

$$E_{pa} (V) = 0.0615 \log[v (V s^{-1})] + 0.3385 \quad (R^2 = 0.9989) \quad (3)$$

Figure 6a exhibited that for $v > 70$ mV s⁻¹, the value of [E_{pa} − E_{pc}]/2 remained essentially unchanged. Hence, at 100 mV s⁻¹ scan rate, the [E_{pa} − E_{pc}]/2 value assume to be 90.5/n_α mV [61], consequently, it was determined that there were 2.29 ≈ 2 transferred electrons (n_α). Therefore, it is established that AA oxidation at the Yb₂O₃.CuO@rGO/GCE surface was a two-electron-transfer system. Overall, the scan rate and pH investigations determined that AA oxidation at the Yb₂O₃.CuO@rGO/GCE surface is a combined two-electrons and two-protons reaction, which is consistent with the literature [13].

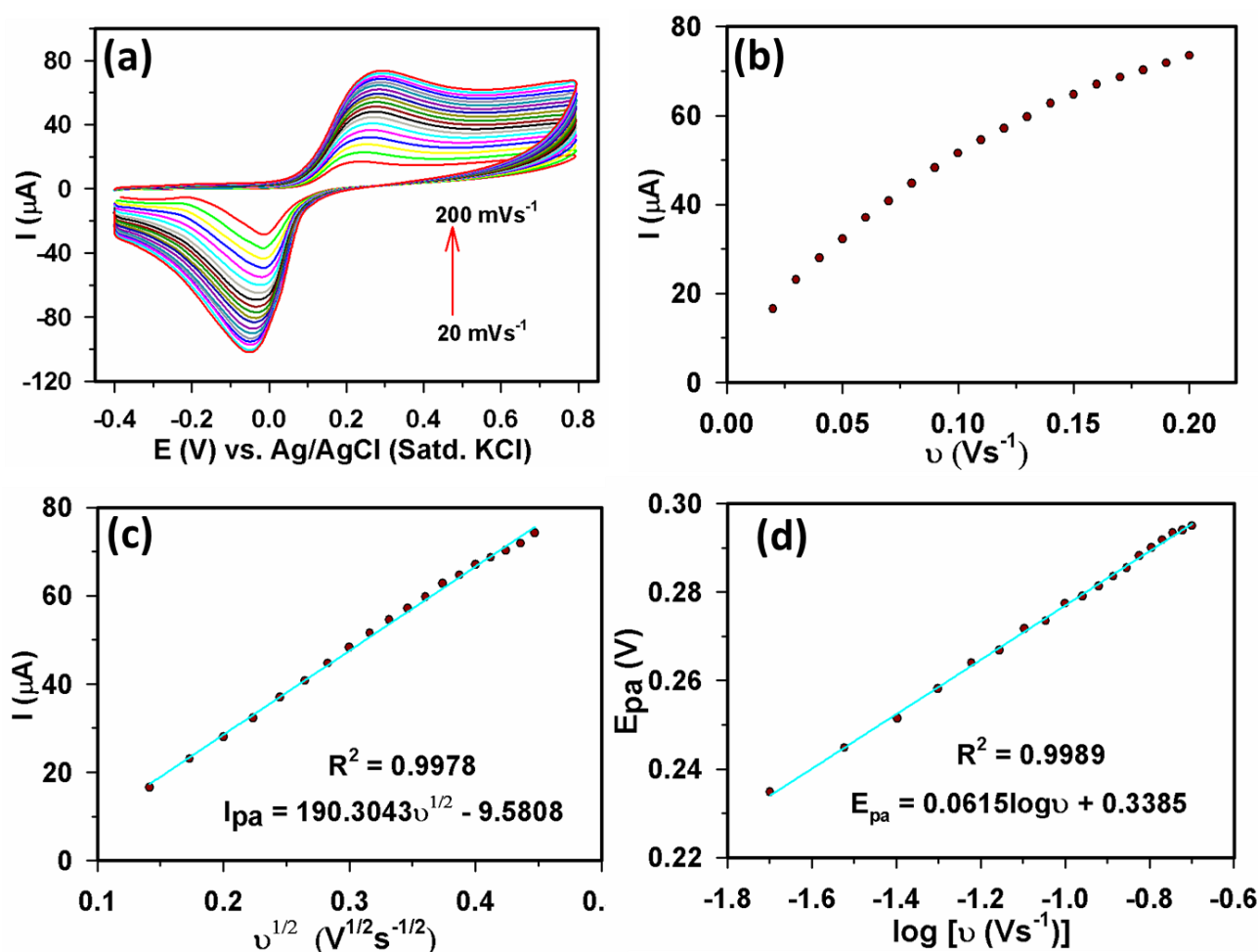


Figure 6. Investigation of scan rate effect of $\text{Yb}_2\text{O}_3.\text{CuO@rGO}/\text{GCE}$ sensor: (a) CVs recorded at different scan rates (20–200 mVs^{-1}) with 40 μM AA in 0.1 M PBS (b) I_{pa} vs. v , (c) I_{pa} vs. \sqrt{v} , and (d) E_{pa} vs. $\log(v)$.

3.2.2. Sensor Parameters Determination

We used amperometry for evaluating the sensor performance of the $\text{Yb}_2\text{O}_3.\text{CuO@rGO}/\text{GCE}$ sensor. An amperometric response was acquired at +0.3 V after adding AA of varying concentrations (0.5–1744 μM) at consecutive time intervals. Figure 7a displays the amperometric responses achieved from the $\text{Yb}_2\text{O}_3.\text{CuO@rGO}/\text{GCE}$ sensor for AA additions. Here, the current response in each AA addition increased to around 95% of its maximum current in just 4 s. Figure 7b shows a linear segment of calibration plot for 0.5–1744 μM AA using the Equation (4).

$$I (\mu\text{A}) = 0.0214 [\text{AA}] (\mu\text{M}) + 0.1527 \quad (R^2 = 0.9989) \quad (4)$$

As a result, the $\text{Yb}_2\text{O}_3.\text{CuO@rGO}/\text{GCE}$ sensor's linear detection range (LDR) was determined to be 0.5–1571 μM . Additionally, the $\text{Yb}_2\text{O}_3.\text{CuO@rGO}/\text{GCE}$ sensor's estimated sensitivity value was found to be $0.4341 \mu\text{A}\mu\text{M}^{-1}\text{cm}^{-2}$ and limit of detection (LOD) and limit of quantification (LOQ) were determined to be $\sim 0.062 \mu\text{M}$ ($S/N = 3$) and $0.1887 \mu\text{M}$, respectively. The sensitivity was calculated using the equation, sensitivity = S/A_{eff} [62], where A_{eff} stands for the surface area of the modified electrode (0.0493 cm^2), as provided in the electronic Supplementary Materials of Figure S1 [19,63,64]. The equations were used to calculate LOD and LOQ are $\text{LOD} = 3.3(S_b/S)$ and $\text{LOQ} = 10(S_b/S)$, respectively [65]; here, S_b (0.000403) stands for relative standard deviation (RSD) related to five blank responses, and S stands for calibration curve's slope.

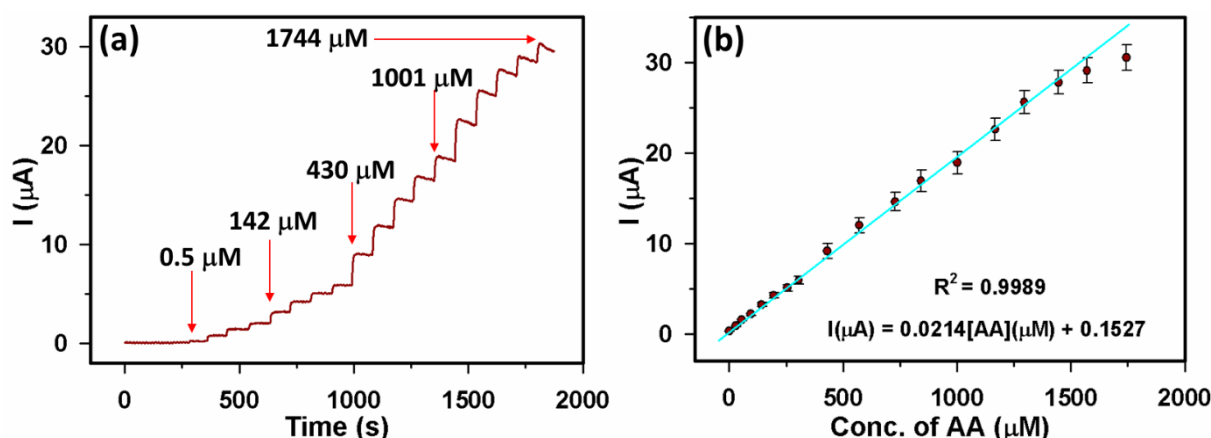


Figure 7. (a) $\text{Yb}_2\text{O}_3.\text{CuO@rGO}/\text{GCE}$ sensor's amperometric response for AA (0.5–1744 μM) at +0.3 V potential, and (b) related calibration plot.

The electrocatalytic performance is dependent on two variables: (i) increase in I_{pa} and (ii) decreased E_{pa} . Hence, attempts have been made to improve the electrocatalytic activity of GCEs by fabricating them using $\text{Yb}_2\text{O}_3.\text{CuO@rGO}$ NC. The achieved results showed that the $\text{Yb}_2\text{O}_3.\text{CuO@rGO}/\text{GCE}$ sensor successfully satisfied both of the aforementioned requirements. Figure 4a showed a substantial negative shift of E_{pa} and a significant increase in I_{pa} from the $\text{Yb}_2\text{O}_3.\text{CuO@rGO}/\text{GCE}$ sensor compared to other electrodes used in this study. We achieved about a three-fold I_{pa} from the $\text{Yb}_2\text{O}_3.\text{CuO@rGO}/\text{GCE}$ compared to a bare GCE during AA oxidation.

3.2.3. Selectivity, Repeatability, Reproducibility, and Stability

To test the $\text{Yb}_2\text{O}_3.\text{CuO@rGO}/\text{GCE}$ sensor's selectivity, we used common interfering chemicals such as uric acid (UA), glucose (Glc), citric acid (CA), dopamine (DA), Cl^- ions, and NO_3^- ions. Here, 90 μM AA and an equal concentration of each interfering chemical were used to record the amperometric response (Figure 8a). While AA addition generated a significant amperometric response, no response was observed for the interfering chemicals. This confirms the selectivity of the $\text{Yb}_2\text{O}_3.\text{CuO@rGO}/\text{GCE}$ assembly during the AA detection. Furthermore, the various sensor characteristics of $\text{Yb}_2\text{O}_3.\text{CuO@rGO}/\text{GCE}$ were also investigated using CV with 40 M AA. A freshly fabricated $\text{Yb}_2\text{O}_3.\text{CuO@rGO}/\text{GCE}$ assembly was employed to measure 40 M AA for the repeatability study shown in Figure 8b. Five runs with a 4.2% RSD and with nearly similar CV responses showed good repeatability. Figure 8c showed the reproducibility study of the $\text{Yb}_2\text{O}_3.\text{CuO@rGO}/\text{GCE}$ assembly that used five newly modified $\text{Yb}_2\text{O}_3.\text{CuO@rGO}/\text{GCE}$ electrodes (E1–E5). The I_{pa} variations in CV responses revealed a 4.7% RSD, demonstrating remarkable reproducibility. In addition, we recorded CV responses every fourth day for a newly modified $\text{Yb}_2\text{O}_3.\text{CuO@rGO}/\text{GCE}$ sensor to assess its stability while keeping it at room temperature. Figure 8d displays the stability investigation bar graph. It demonstrates that the I_{pa} value in CVs was retained at approximately 81% of its initial value after being stored for 20 days at ambient conditions and that the $\text{Yb}_2\text{O}_3.\text{CuO@rGO}/\text{GCE}$ sensor surface remained undamaged.

When the AA molecule touches the $\text{Yb}_2\text{O}_3.\text{CuO@rGO}$ surface, an electro-oxidation reaction occurs. AA molecules release electrons to the conduction-band of the $\text{Yb}_2\text{O}_3.\text{CuO@rGO}$ nanocomposite that ultimately enhance the conductivity of the $\text{Yb}_2\text{O}_3.\text{CuO@rGO}/\text{GCE}$ sensor and, hence, an enhanced CV response can be obtained. In comparison to other AA sensors, the $\text{Yb}_2\text{O}_3.\text{CuO@rGO}/\text{GCE}$ sensor demonstrated a greater sensitivity for AA detection (Table 1) [13,17,39,65–73].

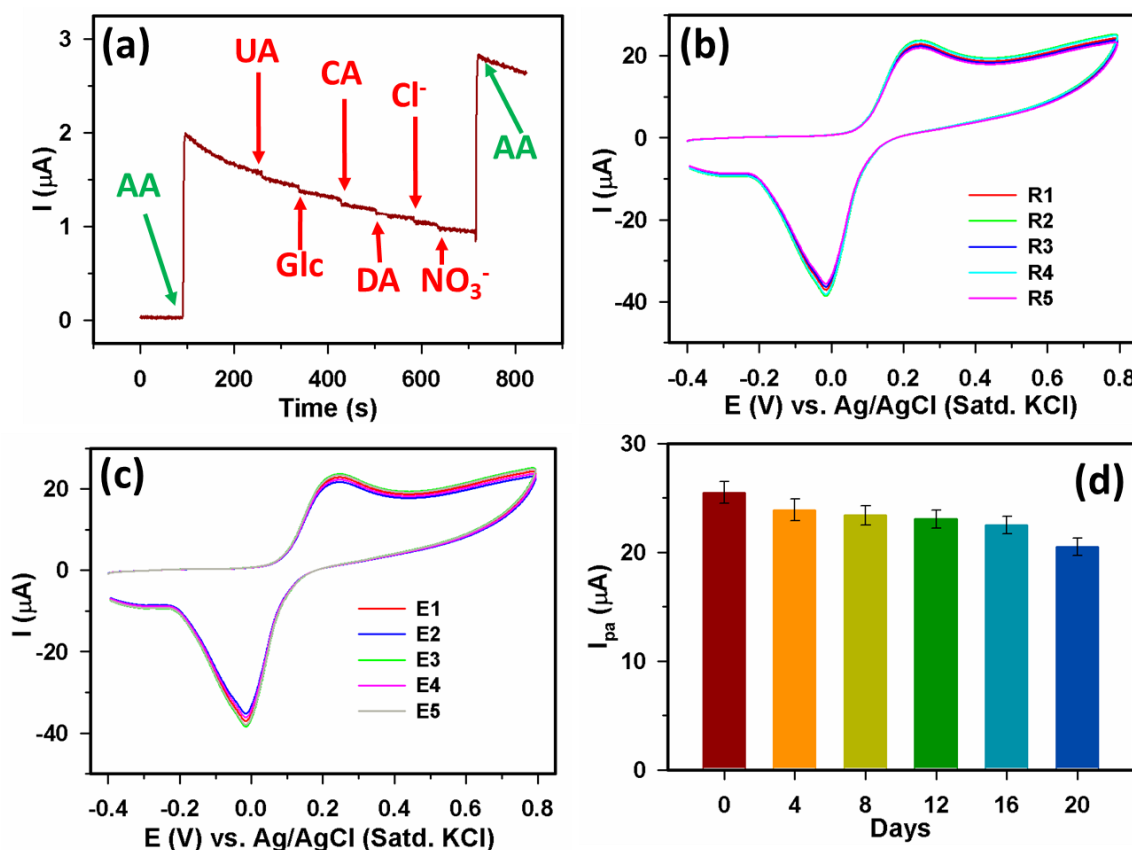


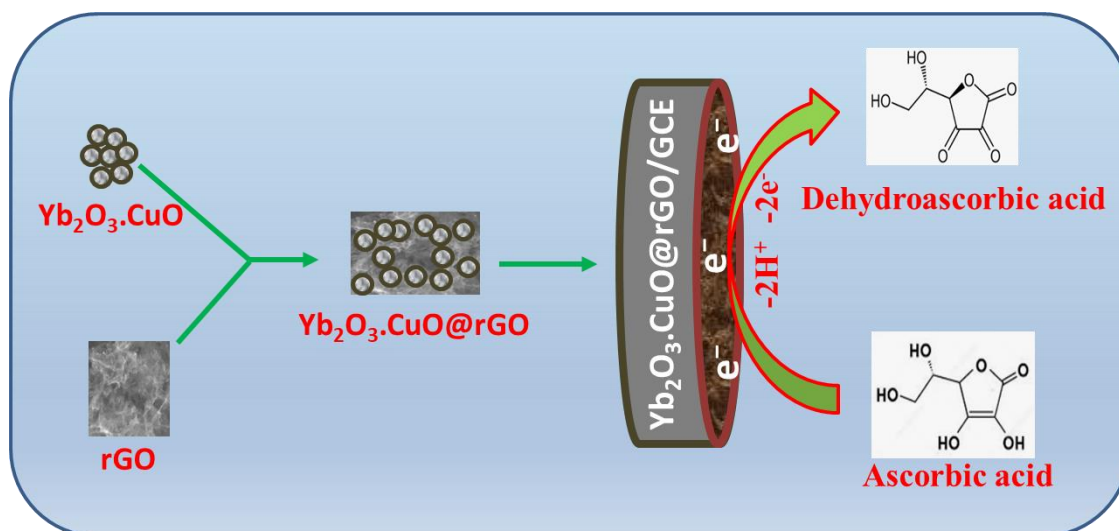
Figure 8. (a) Amperometric (i - t) response at +0.3 V from $\text{Yb}_2\text{O}_3.\text{CuO}@\text{rGO}/\text{GCE}$ sensor upon successive additions of 90 μM of AA, UA, Glc, CA, DA, Cl^- , NO_3^- , and AA, (b) repeatability, (c) reproducibility, and (d) stability investigations.

Table 1. Comparative ascorbic acid sensor performance employing various electrodes.

Electrode	Technique	LDR/ μM	LOD/ μM	Sensitivity/ $\mu\text{A}\mu\text{M}^{-1}\text{cm}^{-2}$	Applied Potential/V	Ref.
PSi-MC/GCE	Amp	0.5–2473	0.03	0.1982	+0.7	[13]
Poly(Py-oPD)/PGE	SWV	1–1000	0.026	-	-	[17]
GO-IL/GCE	Amp	10–4000	3.33	-	+0.8	[66]
DMA/GCE	Amp	25–1650	-	0.178	+0.35	[67]
PoPDoAP/GCE	DPV	100–1000	36.4	$0.0306 \mu\text{A}\mu\text{M}^{-1}$	-	[68]
NFG/Ag/PANI	Amp	10–11,460	8.0	-	+1.2	[69]
PG/GCE	Amp	9.0–2314	6.45	$0.0667 \mu\text{A}\mu\text{M}^{-1}$	-0.01	[70]
ZnO/GCE	Amp	1–800	0.27	$0.1156 \mu\text{A}\mu\text{M}^{-1}$	+0.36	[71]
ERGO/GCE	DPV	500–2000	150	$0.0054 \mu\text{A}\mu\text{M}^{-1}$	-	[72]
PMES/RGO/GCE	DPV	30–100	0.43	-	-	[73]
NPG	Amp	10–1100	2.0	$0.0021 \mu\text{A}\mu\text{M}^{-1}$	+0.3	[74]
GCE/Au@Pd-RGO	DPV	0.01–100	0.002	-	-	[75]
$\text{Yb}_2\text{O}_3.\text{CuO}@\text{rGO}/\text{GCE}$	Amp	0.5–1571	0.062	0.4341	+0.25	This work

PSi-MC = porous silicon-mesoporous carbon; Amp = Amperometry, DMA = N,N Dimethylani-line, GO-IL = Graphene oxide-Ionic liquid, PoPDoAP = Poly(o-phenylenediamine-co-o-aminophenol), NFG = nanoparticles grafted functionalized graphene, PG = pristine graphene, Poly(Py-oPD)/PGE = pencil graphite electrode modified with a molecularly imprinted copolymer of pyrrole and o-phenylenediamine, PMES = Poly(2-(N-morpholine)ethane sulfonic acid), ERGO = electrochemically reduced graphene oxide, and NPG = nanoporous gold.

Considering the experimental findings stated above, we may say that AA oxidation at the $\text{Yb}_2\text{O}_3\cdot\text{CuO@rGO}$ NC is a combined two-electrons and two-protons transfer reaction and, in this AA oxidation, the $\text{Yb}_2\text{O}_3\cdot\text{CuO@rGO}$ NC is exceedingly active. The $\text{Yb}_2\text{O}_3\cdot\text{CuO@rGO}$ /GCE sensor's appropriateness in detecting AA can be attributed to the effective electrode-analyte interaction. Scheme 1 shows a concise model for electrochemical AA oxidation at this novel $\text{Yb}_2\text{O}_3\cdot\text{CuO@rGO}$ /GCE sensor.



Scheme 1. Schematic representation for $\text{Yb}_2\text{O}_3\cdot\text{CuO@rGO}$ /GCE-based ascorbic acid sensor.

3.3. Analyses of Real Samples: AA Detection from Blood Serum and Vitamin C Tablet

The developed suggested $\text{Yb}_2\text{O}_3\cdot\text{CuO@rGO}$ /GCE sensor's efficacy was tested by measuring AA in blood serums and vitamin C tablets utilizing the standard addition method. Firstly, we measured the $\text{Yb}_2\text{O}_3\cdot\text{CuO@rGO}$ /GCE sensor's ($i-t$) response at +0.3 V in 10 mL PBS with 200 μL of undiluted blood serum (BS1) and then three repeated injections of 50 μL 0.01 M AA. Such processes were carried out three times under the same circumstances. Next, we performed the same standard addition procedure using the second blood serum (BS2). Furthermore, we used a dissolved Vitamin C 1000 tablet (Vit-C) from Dallah Pharma Factory, KSA as the real sample, as in our previous report [13]. Finally, we repeated the whole standard addition process using 100 μL of Vitamin C and then three repeated injections of 100 μL 0.01 M AA. Table 2 summarizes the outcomes of the real sample investigations. These results indicate that, with approximately 100% quantitative recovery, this novel $\text{Yb}_2\text{O}_3\cdot\text{CuO@rGO}$ /GCE sensor can be utilized to precisely assess the presence of AA in real samples. Additionally, the measured level of AA in blood serums is within AA levels typically found in adults (28.5–85.2 μM) [7] and, for the Vitamin C tablets, the calculated AA amount was 98.1% of the manufacturer's specification, confirming that the newly-developed $\text{Yb}_2\text{O}_3\cdot\text{CuO@rGO}$ /GCE sensor is appropriately validated.

Table 2. AA Detection from commercial vitamin C tablets and blood serums (BS1 and BS2) using the $\text{Yb}_2\text{O}_3\cdot\text{CuO@rGO}$ /GCE sensor.

Real Samples	Added Std. AA (μM)	Total AA Measured (μM)	AA Measured in Real Samples (μM)	Recovery (%)	RSD (%) ($n = 3$)
BS1	48.8	96.2	46.2	102.4	4.52
	97.6	147.4		103.7	
BS2	48.8	88.1	36.5	105.7	4.13
	97.6	137.0		103.0	
Vit-C	98.0	176.6	82.4	96.1	4.37
	194.2	271.1		97.2	

4. Conclusions

Herein, we successfully synthesized and characterized the $\text{Yb}_2\text{O}_3\cdot\text{CuO}@r\text{GO}$ nanocomposite. This nanocomposite material was then used to design a sensitive, selective, and reusable electrochemical AA sensor. This AA sensor was developed by a facile technique and is able to measure both high and low levels of AA because of its broad linear dynamic range and high sensitivity. Additionally, this AA sensor demonstrated a minimal interference effect, a fast response time, a reasonable limit of detection, excellent stability, reproducibility, and repeatability. These features make it a promising tool for detecting AA. To further validate the $\text{Yb}_2\text{O}_3\cdot\text{CuO}@r\text{GO}/\text{GCE}$ sensor's accuracy, it was tested utilizing blood serums and vitamin C tablets, and the results were consistent and encouraging. Overall, the method of sensor fabrication presented in this study offers a promising platform for developing a highly efficient AA sensor in the future.

Supplementary Materials: The following supporting information can be downloaded at: <https://www.mdpi.com/article/10.3390/bios13060588/s1>, Figure S1: (a) CVs recorded with 5 mM $[\text{Fe}(\text{CN})_6]^{3-/4-}$ in 0.1 M KCl using the $\text{Yb}_2\text{O}_3\cdot\text{CuO}@r\text{GO}/\text{GCE}$ assembly for scan rates ranging from 20 to 120 mVs^{-1} (b) I_{pa} vs. $v^{1/2}$.

Author Contributions: Conceptualization, J.A. and F.A.H.; methodology, J.A., M.F., J.S.A. and M.A.A.; validation, J.A., M.F., J.S.A., M.A.A. and S.A.A.; formal analysis, J.A., M.F. and J.S.A.; investigation, J.A., M.A.A. and F.A.H.; resources, J.S.A. and F.A.H.; data curation, J.A., M.F., J.S.A., M.A.A. and F.A.H.; writing—original draft preparation, J.A.; writing—review and editing, M.F., J.S.A., M.A.A., S.A.A. and F.A.H.; supervision, F.A.H.; project administration, J.S.A. and F.A.H.; funding acquisition, M.A.A. and F.A.H. All authors have read and agreed to the published version of the manuscript.

Funding: This research was funded by the grant no. (NU/IFC/2/SERC/-/15) under the Institutional Funding Committee at Najran University, Kingdom of Saudi Arabia.

Institutional Review Board Statement: The study was conducted according to the guidelines of the ethical standards and approved by the Research Ethics Committee of Najran University (reference No. 010509-023062-DS).

Informed Consent Statement: The verbal informed consent of the participants was obtained.

Data Availability Statement: Data will be available upon request.

Acknowledgments: The authors would like to acknowledge the support of the Deputyship for Research and Innovation-Ministry of Education, Kingdom of Saudi Arabia for this research through a grant (NU/IFC/2/SERC/-/15) under the Institutional Funding Committee at Najran University, Kingdom of Saudi Arabia.

Conflicts of Interest: The authors declare no conflict of interest.

References

1. Bilal, S.; Akbar, A.; Shah, A.U.H.A. Highly Selective and Reproducible Electrochemical Sensing of Ascorbic Acid through a Conductive Polymer Coated Electrode. *Polymers* **2019**, *11*, 346. [CrossRef]
2. Qu, C.; Li, H.; Zhou, S.; Li, G.; Wang, C.; Snyders, R.; Bittencourt, C.; Li, W. Bi 2S_3 /RGO Composite Based Electrochemical Sensor for Ascorbic Acid Detection. *Chemosensors* **2021**, *9*, 190. [CrossRef]
3. Tkachenko, A.B.; Onizhuk, M.O.; Tkachenko, O.S.; Arenas, L.T.; Benvenutti, E.V.; Gushikem, Y.; Panteleimonov, A.V. An Electrochemical Sensor Based on Graphite Electrode Modified with Silica Containing 1-n-Propyl-3-Methylimidazolium Species for Determination of Ascorbic Acid. *Methods Objects Chem. Anal.* **2019**, *14*, 5–14. [CrossRef]
4. Chen, F.; Li, Q.; Yu, Y.; Yang, W.; Shi, F.; Qu, Y. Association of Vitamin C, Vitamin D, Vitamin E and Risk of Bladder Cancer: A Dose-Response Meta-Analysis. *Sci. Rep.* **2015**, *5*, 9599. [CrossRef] [PubMed]
5. Liu, S.; Jiang, X.; Yang, M. Electrochemical Sensing of L-Ascorbic Acid by Using a Glassy Carbon Electrode Modified with a Molybdophosphate Film. *Microchim. Acta* **2019**, *186*, 445. [CrossRef] [PubMed]
6. Mandl, J.; Szarka, A.; Bánhegyi, G. Vitamin C: Update on Physiology and Pharmacology. *Br. J. Pharmacol.* **2009**, *157*, 1097–1110. [CrossRef] [PubMed]
7. Hagel, A.F.; Albrecht, H.; Dauth, W.; Hagel, W.; Vitali, F.; Ganzleben, I.; Schultis, H.W.; Konturek, P.C.; Stein, J.; Neurath, M.F.; et al. Plasma Concentrations of Ascorbic Acid in a Cross Section of the German Population. *J. Int. Med. Res.* **2018**, *46*, 168–174. [CrossRef] [PubMed]

8. Massey, L.K.; Liebman, M.; Kynast-Gales, S.A. Ascorbate Increases Human Oxaluria and Kidney Stone Risk. *J. Nutr.* **2005**, *135*, 1673–1677. [[CrossRef](#)]
9. Lenghor, N.; Jakmunee, J.; Vilen, M.; Sara, R.; Christian, G.D.; Grudpan, K. Sequential Injection Redox or Acid-Base Titration for Determination of Ascorbic Acid or Acetic Acid. *Talanta* **2002**, *58*, 1139–1144. [[CrossRef](#)]
10. Klimczak, I.; Gliszczynska-Swiglo, A. Comparison of UPLC and HPLC Methods for Determination of Vitamin C. *Food Chem.* **2015**, *175*, 100–105. [[CrossRef](#)]
11. Gómez Ruiz, B.; Roux, S.; Courtois, F.; Bonazzi, C. Spectrophotometric Method for Fast Quantification of Ascorbic Acid and Dehydroascorbic Acid in Simple Matrix for Kinetics Measurements. *Food Chem.* **2016**, *211*, 583–589. [[CrossRef](#)] [[PubMed](#)]
12. Morosanova, M.A.; Morosanova, E.I. Silica-Titania Xerogel Doped with Mo,P-Heteropoly Compounds for Solid Phase Spectrophotometric Determination of Ascorbic Acid in Fruit Juices, Pharmaceuticals, and Synthetic Urine. *Chem. Cent. J.* **2017**, *11*, 3. [[CrossRef](#)] [[PubMed](#)]
13. Ahmed, J.; Faisal, M.; Harraz, F.A.; Jalalah, M.; Alsareii, S.A. Porous Silicon-Mesoporous Carbon Nanocomposite Based Electrochemical Sensor for Sensitive and Selective Detection of Ascorbic Acid in Real Samples. *J. Taiwan Inst. Chem. Eng.* **2021**, *125*, 360–371. [[CrossRef](#)]
14. Hameed, S.; Munawar, A.; Khan, W.S.; Mujahid, A.; Ihsan, A.; Rehman, A.; Ahmed, I.; Bajwa, S.Z. Assessing Manganese Nanostructures Based Carbon Nanotubes Composite for the Highly Sensitive Determination of Vitamin C in Pharmaceutical Formulation. *Biosens. Bioelectron.* **2017**, *89*, 822–828. [[CrossRef](#)] [[PubMed](#)]
15. Arabali, V.; Ebrahimi, M.; Abbasghorbani, M.; Gupta, V.K.; Farsi, M.; Ganjali, M.R.; Karimi, F. Electrochemical Determination of Vitamin C in the Presence of NADH Using a CdO Nanoparticle/Ionic Liquid Modified Carbon Paste Electrode as a Sensor. *J. Mol. Liq.* **2016**, *213*, 312–316. [[CrossRef](#)]
16. Tadayon, F.; Vahed, S.; Bagheri, H. Au-Pd/Reduced Graphene Oxide Composite as a New Sensing Layer for Electrochemical Determination of Ascorbic Acid, Acetaminophen and Tyrosine. *Mater. Sci. Eng. C* **2016**, *68*, 805–813. [[CrossRef](#)]
17. Yan, C.; Liu, X.; Zhang, R.; Chen, Y.; Wang, G. A Selective Strategy for Determination of Ascorbic Acid Based on Molecular Imprinted Copolymer of O-Phenylenediamine and Pyrrole. *J. Electroanal. Chem.* **2016**, *780*, 276–281. [[CrossRef](#)]
18. Ahmed, J.; Faisal, M.; Alsareii, S.A.; Harraz, F.A. Highly Sensitive and Selective Non-Enzymatic Uric Acid Electrochemical Sensor Based on Novel Polypyrrole-Carbon Black-Co₃O₄ Nanocomposite. *Adv. Compos. Hybrid Mater.* **2022**, *5*, 920–933. [[CrossRef](#)]
19. Ahmed, J.; Faisal, M.; Jalalah, M.; Alsaiani, M.; Alsareii, S.A.; Harraz, F.A. An Efficient Amperometric Catechol Sensor Based on Novel Polypyrrole-Carbon Black Doped α -Fe₂O₃ Nanocomposite. *Colloids Surfaces A Physicochem. Eng. Asp.* **2021**, *619*, 126469. [[CrossRef](#)]
20. Rahman, M.M.; Ahmed, J.; Asiri, A.M.; Alamry, K.A. Fabrication of a Hydrazine Chemical Sensor Based on Facile Synthesis of Doped NZO Nanostructure Materials. *New J. Chem.* **2020**, *44*, 13018–13029. [[CrossRef](#)]
21. Rahman, M.M.; Ahmed, J.; Asiri, A.M.; Alfaifi, S.Y. Ultra-Sensitive, Selective and Rapid Carcinogenic Bisphenol A Contaminant Determination Using Low-Dimensional Facile Binary Mg-SnO₂ Doped Microcube by Potential Electro-Analytical Technique for the Safety of Environment. *J. Ind. Eng. Chem.* **2022**, *109*, 147–154. [[CrossRef](#)]
22. Mahmoud, B.G.; Khairy, M.; Rashwan, F.A.; Foster, C.W.; Banks, C.E. Self-Assembly of Porous Copper Oxide Hierarchical Nanostructures for Selective Determinations of Glucose and Ascorbic Acid. *RSC Adv.* **2016**, *6*, 14474–14482. [[CrossRef](#)]
23. Wang, X.; Han, Q.; Cai, S.; Wang, T.; Qi, C.; Yang, R.; Wang, C. Excellent Peroxidase Mimicking Property of CuO/Pt Nanocomposites and Their Application as an Ascorbic Acid Sensor. *Analyst* **2017**, *142*, 2500–2506. [[CrossRef](#)]
24. Šljukić, B.R.; Kadara, R.O.; Banks, C.E. Disposable Manganese Oxide Screen Printed Electrodes for Electroanalytical Sensing. *Anal. Methods* **2011**, *3*, 105–109. [[CrossRef](#)] [[PubMed](#)]
25. Zhu, S.; Xie, A.; Wei, B.; Tao, X.; Zhang, J.; Peng, W.; Liu, C.; Gu, L.; Xu, C.; Luo, S. Construction and Application of a Nonenzymatic Ascorbic Acid Sensor Based on a NiO_{1.0}/Polyaniline_{3.0} hybrid. *New J. Chem.* **2020**, *44*, 9288–9297. [[CrossRef](#)]
26. Yin, Y.; Zhao, J.; Qin, L.; Yang, Y.; He, L. Synthesis of an Ordered Nanoporous Fe₂O₃/Au Film for Application in Ascorbic Acid Detection. *RSC Adv.* **2016**, *6*, 63358–63364. [[CrossRef](#)]
27. Pan, Y.; Zuo, J.; Hou, Z.; Huang, Y.; Huang, C. Preparation of Electrochemical Sensor Based on Zinc Oxide Nanoparticles for Simultaneous Determination of AA, DA, and UA. *Front. Chem.* **2020**, *8*, 592538. [[CrossRef](#)]
28. Zhang, X.; Yu, S.; He, W.; Uyama, H.; Xie, Q.; Zhang, L.; Yang, F. Electrochemical Sensor Based on Carbon-Supported NiCoO₂ Nanoparticles for Selective Detection of Ascorbic Acid. *Biosens. Bioelectron.* **2014**, *55*, 446–451. [[CrossRef](#)]
29. Alam, M.M.; Asiri, A.M.; Rahman, M.M.; Islam, M.A. Selective Detection of Ascorbic Acid with Wet-Chemically Prepared CdO/SnO₂/V₂O₅ Micro-Sheets by Electrochemical Approach. *SN Appl. Sci.* **2020**, *2*, 1953. [[CrossRef](#)]
30. Xing, R.; Sheng, K.; Xu, L.; Liu, W.; Song, J.; Song, H. Three-Dimensional In₂O₃-CuO Inverse Opals: Synthesis and Improved Gas Sensing Properties towards Acetone. *RSC Adv.* **2016**, *6*, 57389–57395. [[CrossRef](#)]
31. Purbia, R.; Kwon, Y.M.; Choi, S.Y.; Kim, S.H.; Lee, Y.S.; Ahi, Z.B.; Park, H.; Baik, J.M. A Thermodynamic Approach toward Selective and Reversible Sub-Ppm H₂S Sensing Using Ultra-Small CuO Nanorods Impregnated with Nb₂O₅ nanoparticles. *J. Mater. Chem. A* **2021**, *9*, 17425–17433. [[CrossRef](#)]
32. Hossain, R.; Hassan, K.; Sahajwalla, V. Utilising Problematic Waste to Detect Toxic Gas Release in the Environment: Fabricating a NiO Doped CuO Nanoflake Based Ammonia Sensor from e-Waste. *Nanoscale Adv.* **2022**, *4*, 4066–4079. [[CrossRef](#)] [[PubMed](#)]
33. Chen, Y.; Shen, Z.; Jia, Q.; Zhao, J.; Zhao, Z.; Ji, H. A CuO-ZnO Nanostructured p-n Junction Sensor for Enhanced N-Butanol Detection. *RSC Adv.* **2016**, *6*, 2504–2511. [[CrossRef](#)]

34. Hussain, M.M.; Hussain, M.M.; Hussain, M.M.; Asiri, A.M.; Rahman, M.M.; Rahman, M.M.; Hussain, M.M. A Non-Enzymatic Electrochemical Approach for L-Lactic Acid Sensor Development Based on CuO-MWCNT Nanocomposites Modified with a Nafion Matrix. *New J. Chem.* **2020**, *44*, 9775–9787. [\[CrossRef\]](#)
35. Tobaldi, D.M.; Espro, C.; Leonardi, S.G.; Lajaunie, L.; Seabra, M.P.; Calvino, J.J.; Marini, S.; Labrincha, J.A.; Neri, G. Photo-Electrochemical Properties of CuO-TiO₂ heterojunctions for Glucose Sensing. *J. Mater. Chem. C* **2020**, *8*, 9529–9539. [\[CrossRef\]](#)
36. Sun, G.J.; Choi, S.W.; Katoch, A.; Wu, P.; Kim, S.S. Bi-Functional Mechanism of H₂S Detection Using CuO-SnO₂ Nanowires. *J. Mater. Chem. C* **2013**, *1*, 5454–5462. [\[CrossRef\]](#)
37. Rahman, M.M. Rapid and Sensitive Detection of Selective 1,2-Diaminobenzene Based on Facile Hydrothermally Prepared Doped Co₃O₄/Yb₂O₃ Nanoparticles. *PLoS ONE* **2021**, *16*, e0246756. [\[CrossRef\]](#)
38. Rahman, M.M.; Alam, M.M.; Asiri, A.M.; Islam, M.A. Ethanol Sensor Development Based on Ternary-Doped Metal Oxides (CdO/ZnO/Yb₂O₃) Nanosheets for Environmental Safety. *RSC Adv.* **2017**, *7*, 22627–22639. [\[CrossRef\]](#)
39. Rahman, M.M.; Alam, M.M.; Asiri, A.M.; Awual, M.R. Fabrication of 4-Aminophenol Sensor Based on Hydrothermally Prepared ZnO/Yb₂O₃ Nanosheets. *New J. Chem.* **2017**, *41*, 9159–9169. [\[CrossRef\]](#)
40. Umar, A.; Ibrahim, A.A.; Kumar, R.; Almas, T.; Al-Assiri, M.S.; Baskoutas, S. Nitroaniline Chemo-Sensor Based on Bitter Gourd Shaped Ytterbium Oxide (Yb₂O₃) Doped Zinc Oxide (ZnO) Nanostructures. *Ceram. Int.* **2019**, *45*, 13825–13831. [\[CrossRef\]](#)
41. Wang, Y.; Liu, L.; Sun, F.; Li, T.; Zhang, T.; Qin, S. Humidity-Insensitive NO₂ Sensors Based on SnO₂/RGO Composites. *Front. Chem.* **2021**, *9*, 681313. [\[CrossRef\]](#) [\[PubMed\]](#)
42. Gupta, M.; Hawari, H.F.; Kumar, P.; Burhanudin, Z.A.; Tansu, N. Functionalized Reduced Graphene Oxide Thin Films for Ultrahigh CO₂ Gas Sensing Performance at Room Temperature. *Nanomaterials* **2021**, *11*, 623. [\[CrossRef\]](#) [\[PubMed\]](#)
43. Jiang, W.; Chen, X.; Wang, T.; Li, B.; Zeng, M.; Yang, J.; Hu, N.; Su, Y.; Zhou, Z.; Yang, Z. Enhancing Room-Temperature NO₂ gas Sensing Performance Based on a Metal Phthalocyanine/Graphene Quantum Dot Hybrid Material. *RSC Adv.* **2021**, *11*, 5618–5628. [\[CrossRef\]](#) [\[PubMed\]](#)
44. Feizollahi, A.; Rafati, A.A.; Assari, P.; Asadpour Joghani, R. Development of an Electrochemical Sensor for the Determination of Antibiotic Sulfamethazine in Cow Milk Using Graphene Oxide Decorated with Cu-Ag Core-Shell Nanoparticles. *Anal. Methods* **2021**, *13*, 910–917. [\[CrossRef\]](#)
45. Yu, H.; Guo, W.; Lu, X.; Xu, H.; Yang, Q.; Tan, J.; Zhang, W. Reduced Graphene Oxide Nanocomposite Based Electrochemical Biosensors for Monitoring Foodborne Pathogenic Bacteria: A Review. *Food Control* **2021**, *127*, 108117. [\[CrossRef\]](#)
46. Fauzi, A.S.A.; Hamidah, N.L.; Kitamura, S.; Kodama, T.; Sonda, K.; Putri, G.K.; Shinkai, T.; Ahmad, M.S.; Inomata, Y.; Quitain, A.T.; et al. Electrochemical Detection of Ethanol in Air Using Graphene Oxide Nanosheets Combined with Au-WO₃. *Sensors* **2022**, *22*, 3194. [\[CrossRef\]](#)
47. Wu, S.; Liang, Y.; Xu, Y.; Tong, Y.; Chen, Y.; Chen, X. Graphene-Based Electrochemical Sensor for Detection of Hepatocellular Carcinoma Markers. *Front. Chem.* **2022**, *10*, 883627. [\[CrossRef\]](#)
48. Boroujerdi, R.; Paul, R. Graphene-Based Electrochemical Sensors for Psychoactive Drugs. *Nanomaterials* **2022**, *12*, 2250. [\[CrossRef\]](#)
49. Fu, L.; Mao, S.; Chen, F.; Zhao, S.; Su, W.; Lai, G.; Yu, A.; Lin, C.-T. Graphene-Based Electrochemical Sensors for Antibiotic Detection in Water, Food and Soil: A Scientometric Analysis in CiteSpace (2011–2021). *Chemosphere* **2022**, *297*, 134127. [\[CrossRef\]](#)
50. Saravanan, T.; Anandan, P.; Shanmugam, M.; Azhagurajan, M.; Mohamed Ismail, M.; Arivanandhan, M.; Hayakawa, Y.; Jayavel, R. Facile Synthesis of Yb₂O₃-Graphene Nanocomposites for Enhanced Energy and Environmental Applications. *Polym. Bull.* **2020**, *77*, 3891–3906. [\[CrossRef\]](#)
51. Aftab, U.; Tahira, A.; Mazzaro, R.; Abro, M.I.; Baloch, M.M.; Willander, M.; Nur, O.; Yu, C.; Ibupoto, Z.H. The Chemically Reduced CuO-Co₃O₄ Composite as a Highly Efficient Electrocatalyst for Oxygen Evolution Reaction in Alkaline Media. *Catal. Sci. Technol.* **2019**, *9*, 6274–6284. [\[CrossRef\]](#)
52. Baig, N.; Saleh, T.A. Superhydrophobic Polypropylene Functionalized with Nanoparticles for Efficient Fast Static and Dynamic Separation of Spilled Oil from Water. *Glob. Chall.* **2019**, *3*, 1800115. [\[CrossRef\]](#) [\[PubMed\]](#)
53. Gongalsky, M.B.; Kargina, J.V.; Cruz, J.F.; Sánchez-Royo, J.F.; Chirvony, V.S.; Osminkina, L.A.; Sailor, M.J. Formation of Si/SiO₂ Luminescent Quantum Dots From Mesoporous Silicon by Sodium Tetraborate/Citric Acid Oxidation Treatment. *Front. Chem.* **2019**, *7*, 165. [\[CrossRef\]](#) [\[PubMed\]](#)
54. Yu, L.; Zhang, P.; Dai, H.; Chen, L.; Ma, H.; Lin, M.; Shen, D. An Electrochemical Sensor Based on Co₃O₄ Nanosheets for Lead Ions Determination. *RSC Adv.* **2017**, *7*, 39611–39616. [\[CrossRef\]](#)
55. Eslami, A.; Juibari, N.M.; Hosseini, S.G.; Abbasi, M. Synthesis and Characterization of CuO Nanoparticles by the Chemical Liquid Deposition Method and Investigation of Its Catalytic Effect on the Thermal Decomposition of Ammonium Perchlorate. *Cent. Eur. J. Energetic Mater.* **2017**, *14*, 152–168. [\[CrossRef\]](#)
56. Rahman, M.M.; Ahmed, J.; Asiri, A.M. Ultra-Sensitive, Selective, and Rapid Carcinogenic 1,2-Diaminobenzene Chemical Determination Using Sol-Gel Coating Low-Dimensional Facile CuS Modified-CNT Nanocomposites by Electrochemical Approach. *Microchem. J.* **2022**, *175*, 107230. [\[CrossRef\]](#)
57. Cao, Z.; An, S.; Song, X. Effect of Thermal Treatment at High Temperature on Phase Stability and Transformation of Yb₂O₃ and Y₂O₃ Co-Doped ZrO₂ Ceramics. *Sci. Rep.* **2022**, *12*, 9955. [\[CrossRef\]](#)
58. Wang, J.; Salihi, E.C.; Šiller, L. Green Reduction of Graphene Oxide Using Alanine. *Mater. Sci. Eng. C* **2017**, *72*, 1–6. [\[CrossRef\]](#)
59. El-Raheem, H.A.; Hassan, R.Y.A.; Khaled, R.; Farghali, A.; El-Sherbiny, I.M. New Sensing Platform of Poly(Ester-Urethane)Urea Doped with Gold Nanoparticles for Rapid Detection of Mercury Ions in Fish Tissue. *RSC Adv.* **2021**, *11*, 31845–31854. [\[CrossRef\]](#)

60. Ahmed, J.; Rahman, M.M.; Siddiquey, I.A.; Asiri, A.M.; Hasnat, M.A. Efficient Bisphenol-A Detection Based on the Ternary Metal Oxide (TMO) Composite by Electrochemical Approaches. *Electrochim. Acta* **2017**, *246*, 597–605. [[CrossRef](#)]
61. Ahmed, J.; Rahman, M.M.; Siddiquey, I.A.; Asiri, A.M.; Hasnat, M.A. Efficient Hydroquinone Sensor Based on Zinc, Strontium and Nickel Based Ternary Metal Oxide (TMO) Composites by Differential Pulse Voltammetry. *Sens. Actuators B Chem.* **2018**, *256*, 383–392. [[CrossRef](#)]
62. Ahmed, J.; Faisal, M.; Jalalah, M.; Alsareii, S.A.; Harraz, F.A. Novel Polypyrrole-Carbon Black Doped ZnO Nanocomposite for Efficient Amperometric Detection of Hydroquinone. *J. Electroanal. Chem.* **2021**, *898*, 115631. [[CrossRef](#)]
63. Ahmed, J.; Faisal, M.; Alsareii, S.A.; Jalalah, M.; Harraz, F.A. A Novel Gold-Decorated Porous Silicon-Poly(3-Hexylthiophene) Ternary Nanocomposite as a Highly Sensitive and Selective Non-Enzymatic Dopamine Electrochemical Sensor. *J. Alloys Compd.* **2023**, *931*, 167403. [[CrossRef](#)]
64. Ahmed, J.; Rashed, M.A.; Faisal, M.; Harraz, F.A.; Jalalah, M.; Alsareii, S.A. Novel SWCNTs-Mesoporous Silicon Nanocomposite as Efficient Non-Enzymatic Glucose Biosensor. *Appl. Surf. Sci.* **2021**, *552*, 149477. [[CrossRef](#)]
65. Ahmed, J.; Faisal, M.; Alsareii, S.A.; Jalalah, M.; Alsaiari, M.; Harraz, F.A. Mn₂O₃ Nanoparticle-Porous Silicon Nanocomposite Based Amperometric Sensor for Sensitive Detection and Quantification of Acetaminophen in Real Samples. *Ceram. Int.* **2023**, *49*, 933–943. [[CrossRef](#)]
66. Xu, C.; Liu, B.; Ning, W.; Wang, X. Highly Sensitive Ascorbic Acid Sensor Based on Ionic Liquid Functionalized Graphene Oxide Nanocomposite. *Int. J. Electrochem. Sci.* **2019**, *14*, 1670–1683. [[CrossRef](#)]
67. Roy, P.R.; Saha, M.S.; Okajima, T.; Ohsaka, T. Electrooxidation and Amperometric Detection of Ascorbic Acid at GC Electrode Modified by Electropolymerization of N,N-Dimethylaniline. *Electroanalysis* **2004**, *16*, 289–297. [[CrossRef](#)]
68. Kong, Y.; Shan, X.; Ma, J.; Chen, M.; Chen, Z. A Novel Voltammetric Sensor for Ascorbic Acid Based on Molecularly Imprinted Poly(o-Phenylenediamine-Co-o-Aminophenol). *Anal. Chim. Acta* **2014**, *809*, 54–60. [[CrossRef](#)]
69. Salahandish, R.; Ghaffarinejad, A.; Naghib, S.M.; Niyazi, A.; Majidzadeh-A, K.; Janmaleki, M.; Sanati-Nezhad, A. Sandwich-Structured Nanoparticles-Grafted Functionalized Graphene Based 3D Nanocomposites for High-Performance Biosensors to Detect Ascorbic Acid Biomolecule. *Sci. Rep.* **2019**, *9*, 1226. [[CrossRef](#)]
70. Qi, S.; Zhao, B.; Tang, H.; Jiang, X. Determination of Ascorbic Acid, Dopamine, and Uric Acid by a Novel Electrochemical Sensor Based on Pristine Graphene. *Electrochim. Acta* **2015**, *161*, 395–402. [[CrossRef](#)]
71. Zhu, H.; Xu, G. Electrochemical Determination of Ascorbic Acid Based on Hydrothermal Synthesized ZnO Nanoparticles. *Int. J. Electrochem. Sci.* **2017**, *12*, 3873–3882. [[CrossRef](#)]
72. Yang, L.; Liu, D.; Huang, J.; You, T. Simultaneous Determination of Dopamine, Ascorbic Acid and Uric Acid at Electrochemically Reduced Graphene Oxide Modified Electrode. *Sens. Actuators B Chem.* **2014**, *193*, 166–172. [[CrossRef](#)]
73. Zhang, K.; Zhang, N.; Zhang, L.; Wang, H.; Shi, H.; Liu, Q. Simultaneous Voltammetric Detection of Dopamine, Ascorbic Acid and Uric Acid Using a Poly(2-(N-Morpholine)Ethane Sulfonic Acid)/RGO Modified Electrode. *RSC Adv.* **2018**, *8*, 5280–5285. [[CrossRef](#)] [[PubMed](#)]
74. Kumar, A.; Furtado, V.L.; Gonçalves, J.M.; Bannitz-Fernandes, R.; Netto, L.E.S.; Araki, K.; Bertotti, M. Amperometric Microsensor Based on Nanoporous Gold for Ascorbic Acid Detection in Highly Acidic Biological Extracts. *Anal. Chim. Acta* **2020**, *1095*, 61–70. [[CrossRef](#)] [[PubMed](#)]
75. Jiang, J.; Du, X. Sensitive Electrochemical Sensors for Simultaneous Determination of Ascorbic Acid, Dopamine, and Uric Acid Based on Au@Pd-Reduced Graphene Oxide Nanocomposites. *Nanoscale* **2014**, *6*, 11303–11309. [[CrossRef](#)] [[PubMed](#)]

Disclaimer/Publisher’s Note: The statements, opinions and data contained in all publications are solely those of the individual author(s) and contributor(s) and not of MDPI and/or the editor(s). MDPI and/or the editor(s) disclaim responsibility for any injury to people or property resulting from any ideas, methods, instructions or products referred to in the content.